

**Long-range interactions between polar alkali-metal diatoms in external electric fields**M. Lepers,<sup>1,\*</sup> R. Vexiau,<sup>1</sup> M. Aymar,<sup>1</sup> N. Bouloufa-Maafa,<sup>1,2</sup> and O. Dulieu<sup>1</sup><sup>1</sup>*Laboratoire Aimé Cotton, CNRS/Université Paris-Sud/ENS-Cachan, Bâtiment 505, Campus d'Orsay, 91405 Orsay, France*<sup>2</sup>*UFR Sciences et Techniques, Université Cergy-Pontoise, 95000 Cergy-Pontoise, France*

(Received 24 May 2013; revised manuscript received 9 August 2013; published 26 September 2013)

We computed the long-range interactions between two identical polar alkali molecules in their rovibronic ground level for all ten species involving Li, Na, K, Rb, and Cs, using accurate quantum chemistry results combined with available spectroscopic data. A huge van der Waals interaction is found for eight species in free space. The competition of the van der Waals interaction with the dipole-dipole interaction induced by an external electric field parallel or perpendicular to the intermolecular axis is investigated by varying the electric-field magnitude and the intermolecular distance. Our calculations predict a regime with the mutual orientation of the two molecules but with no preferential direction in the laboratory frame. A mechanism for the stimulated one-photon radiative association of a pair of ultracold polar molecules into ultracold tetramers is proposed, which would open the way towards the optical manipulation of ultracold polyatomic molecules.

DOI: 10.1103/PhysRevA.88.032709

PACS number(s): 34.20.Gj, 34.50.Cx

**I. INTRODUCTION**

The dynamics of ultracold quantum gases composed of atoms or molecules with extremely low translational energy  $E_t/k_B \ll 1$  mK is dominated by the long-range mutual interactions between particles. Such gases are currently routinely produced in various laboratories worldwide, and many applications are foreseen [1,2]. When they are trapped in external potentials created by electromagnetic fields, they offer unique opportunities to study fundamental few-body dynamics in atomic and molecular physics [3]. The unprecedented capability to simultaneously control the internal and external degrees of freedom of the particles also opens the way to the quantum simulation of Hamiltonians describing many-body physical phenomena like low-temperature Fermi fluids or artificial gauge fields [4,5]. When the particles possess an intrinsic magnetic or electric dipole moment, they interact through strong long-range anisotropic forces, i.e., depending on their mutual orientation, which strongly modifies the dynamics of the quantum gas [6,7] and enhances stereochemical properties of ultracold bimolecular reactions [8].

The recent production of ultracold heteronuclear alkali-metal dimers in their lowest rovibronic [9,10] and hyperfine levels [11] stimulates many studies in this perspective. The permanent electric dipole moment (PEDM)  $d_0$  of such (polar) molecules in their own frame allows for manipulating them with static electric fields [12,13] and electromagnetic fields [8,14–16]. Such studies require a detailed modeling of the molecule-molecule long-range interactions inside the quantum gas with or without the presence of external fields [17,18]. The most spectacular experimental achievements on ultracold dipolar molecular gases have been performed on KRb molecules [8,9,11,19] which motivated a wealth of theoretical investigations on this species [17,20–23]. An accurate description of long-range interactions involving the other heteronuclear alkali diatoms is strongly needed since they draw rising attention [24–32]. Considering two identical polar molecules at large distances  $R$  (in atomic units

1 a.u.  $\equiv a_0 = 0.052917721092$  nm) between their individual centers of mass (c.m.) connected by the  $z$  axis and with polar angles  $(\theta_i, \phi_i)$ ,  $i = 1, 2$ , with respect to the  $z$  axis, their mutual long-range dipole-dipole interaction is conveniently written in the coordinate system associated with the tetramer (T-CS) based on the  $z$  axis,

$$V_{\text{dd}}(R) = -\frac{d_0^2}{R^3} [2 \cos \theta_1 \cos \theta_2 - \sin \theta_1 \sin \theta_2 \cos(\phi_2 - \phi_1)]. \quad (1)$$

(The atomic units of energy, where 1 a.u.  $\equiv 2\text{Ry} = 219474.63137078$  cm<sup>-1</sup>, will be used throughout the paper unless otherwise stated.) In the range of distances investigated here ( $R \gtrsim 30$  a.u.), it is easy to check that the energy of the mechanical rotation between the two molecules and thus the corresponding rotational couplings are small compared to the van der Waals (vdW) interaction and to the rotational energy of the individual molecules, so that the main features of the system can be captured in the T-CS.

In this paper, we compute the long-range interactions between two identical bosonic polar alkali ground-state molecules both in free space (Secs. II and III) and as a function of the magnitude of an external electric field parallel or perpendicular to the  $z$  axis (Sec. IV). We use the stationary perturbation theory as in our previous investigations on atom-molecule systems [33–37]. In free space, we found that the vdW interaction varying as  $-C_6/R^6$  is characterized by  $C_6$  coefficients that are three orders of magnitude larger than those for alkali atoms, in agreement with the results of Ref. [38], which uses a different method. The isotropic vdW interaction competes with the expected anisotropic dipole-dipole interaction induced by one molecule on the other or by an external electric field  $\mathcal{E}$  [14,28]. Among the ten species built from Li, Na, K, Rb, and Cs atoms, we show that the interactions for KRb and LiNa, which possess the smallest PEDMs of the series, i.e., 0.56 and 0.61 D, respectively [39], behave differently from species with a larger PEDM, ranging from 1.2 D, for RbCs to 5.5 D for LiCs [39]. For the latter molecules, our calculations predict for critical values of  $R$  and  $\mathcal{E}$  the mutual orientation of the two molecules, but with

\*maxence.lepers@u-psud.fr

no preferential direction in the laboratory frame, i.e., no anisotropy of their interaction. Our work complements the recent one by Byrd *et al.* [18], where the authors investigated the long-range interaction between two bialkali ground-state polar molecules aligned by a strong external electric field in the head-to-tail or side-by-side configurations in the laboratory frame. Section V presents a prospective discussion about the possibility to create ultracold ground-state polar tetramers by stimulated one-photon radiative association of a pair of ultracold polar bialkali molecules. Finally, Sec. VI contains more general conclusions and prospects.

## II. CALCULATION OF $C_6$ COEFFICIENTS IN FREE SPACE

In the lowest rovibrational level ( $v = 0$ ,  $j = 0$ ) of the electronic ground state  $X^1\Sigma_g^+$  (denoted hereafter as state  $|0\rangle$ ), the molecules have no PEDM in the T-CS. Their interaction energy  $V_{j_1 j_2}(R)$  is determined by the operator  $\hat{V}_{dd}$  taken at the second order of the perturbation expansion, i.e.,  $-C_6/R^6$ . The  $C_6$  coefficients are expressed in terms of dynamic dipole polarizabilities at imaginary frequencies [40],

$$C_6 = \frac{3}{\pi} \int_0^{+\infty} d\omega [\alpha(i\omega)]^2, \quad (2)$$

where  $\alpha(i\omega)$  is the isotropic polarizability of the rovibronic ground level  $|0\rangle$ , expressed as a sum over all excited levels  $|n\rangle$  accessible by dipolar transition,

$$\alpha(i\omega) = \frac{2}{3} \sum_{n \neq 0} \frac{\omega_{n0} d_{n0}^2}{\omega_{n0}^2 + \omega^2}. \quad (3)$$

In Eq. (3),  $\omega_{n0}$  and  $d_{n0}$  are, respectively, the transition energies and transition dipole moments between  $|n\rangle$  and  $|0\rangle$ , which were extracted from a combination of accurate semiempirical potential energy curves (PECs) and electronic transition dipole moments (TDMs) computed in our group [39,41] and available spectroscopic PECs (Table I). The wave functions for the rovibrational levels and for the dissociation continua were computed using our code based on the mapped Fourier grid Hamiltonian method [42]. The details of our calculations are given in Ref. [43], and will be the subject of a future article.

TABLE I. Permanent dipole moment  $d_0$  (1 a.u. = 2.54158059 D) and rotational constant  $B_0$  for each ground-state molecule in the  $v = 0$  level, obtained after averaging on the  $v = 0$  radial wave function related to the experimental potential energy curve given in the reference in the second column.

Molecule	Ref.	$d_0$ (a.u.)	$B_0$ (cm $^{-1}$ )
$^{23}\text{Na}^{133}\text{Cs}$	[44]	1.845	0.058
$^7\text{Li}^{133}\text{Cs}$	[45]	2.201	0.187
$^{23}\text{Na}^{87}\text{Rb}$	[46]	1.304	0.070
$^7\text{Li}^{87}\text{Rb}$	[47]	1.645	0.215
$^7\text{Li}^{39}\text{K}$	[48]	1.410	0.256
$^{23}\text{Na}^{39}\text{K}$	[49]	1.095	0.095
$^{39}\text{K}^{133}\text{Cs}$	[50]	0.724	0.030
$^{87}\text{Rb}^{133}\text{Cs}$	[51]	0.490	0.016
$^{39}\text{K}^{87}\text{Rb}$	[52]	0.242	0.038
$^7\text{Li}^{23}\text{Na}$	[53]	0.223	0.374

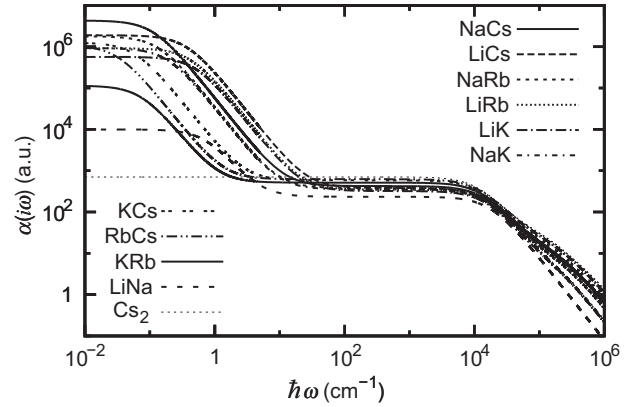


FIG. 1. Dynamic isotropic dipole polarizabilities as functions of the imaginary frequency for the ten heteronuclear bialkali molecules. We also plotted the polarizability of the homonuclear molecule  $\text{Cs}_2$  as a reference [34].

For the ten bialkali heteronuclear species, the polarizability  $\alpha(i\omega)$ , plotted on Fig. 1 in log-log scale, shows two plateaus. The first one, located in the low-frequency region ( $\hbar\omega \approx 0.01$ – $1$  cm $^{-1}$ ), is due to the predominance of the purely rotational transition ( $v = 0, j = 0$ )  $\rightarrow$  ( $v = 0, j = 1$ ) within the lowest electronic state  $X$  in Eq. (3) over all other transitions toward ground-state excited vibrational levels. The height of this plateau is strikingly different from one molecule to another, as shown by its approximate expression considering only the main transition  $\alpha(0) = d_0^2/3B_0$ , where the rotational constant  $B_0$  of the  $X^1\Sigma_g^+$ ,  $v = 0$  level and  $d_0$  are expressed in atomic units. Once  $\hbar\omega$  exceeds this transition energy,  $\alpha(i\omega)$  varies as  $\omega^{-2}$  [Eq. (3)] to reach the next plateau corresponding to the contribution of the transitions toward levels of the excited electronic states. This plateau extends up to  $\hbar\omega \approx 10^4$  cm $^{-1}$  for all species, which reflects (i) that the main contribution to the polarizability comes from the lowest excited electronic states and (ii) that all species have similar electronic excitation energies. Then the polarizability varies as  $\omega^{-2}$  up to  $\hbar\omega \approx 10^5$  cm $^{-1}$ , where the influence of the core electrons on the polarizability produces different slopes for  $\alpha$ . Beyond this range, the polarizability decreases again as  $\omega^{-2}$ .

The existence of those two distinct plateaus allows us to express the  $C_6$  coefficient as the sum of three terms [27],

$$C_6 = C_6^g + C_6^e + C_6^{g-e}, \quad (4)$$

where  $C_6^g$  denotes the contribution of the purely rotational transition inside the ground electronic state (if we neglect transitions to higher vibrational levels),  $C_6^e$  denotes the contribution of transitions to electronically excited states, and where  $C_6^{g-e}$  is a crossed contribution. Our results for all those contributions and for the ten heteronuclear molecules are given in Table II, and they are compared to available literature values. Just like the dynamic polarizabilities, the  $C_6$  coefficients vary dramatically from one molecule to another, ranging from a few thousand atomic units for LiNa and KRb to a few million atomic units for NaCs. Such differences ensue from the ground-state contribution, which can be expressed to a very good approximation as  $C_6^g \approx d_0^4/6B_0$ . Eight molecules out of the ten, which are characterized by a strong PEDM, interact through a

TABLE II. The different contributions to the  $C_6$  coefficient [see Eq. (4)] from two identical ground-state bialkali heteronuclear molecules in their lowest rovibrational levels. In Ref. [38],  $C_6^g$ ,  $C_6^e$ , and  $C_6^{g-e}$  are denoted  $C_6^{\text{rot}}$ ,  $C_6^{\text{disp}}$ , and  $C_6^{\text{ind}}$ , respectively, in [27], our  $C_6^{g-e}$  is called  $C_6^{\text{inf}}$ , and in [18], our  $C_6^e$  and  $C_6^{g-e}$  are  $W_{6000}^{(2,\text{DISP})}$  and  $W_{6000}^{(2)} - W_{6000}^{(2,\text{DIS})}$ , respectively. In addition Ref. [55] gives  $C_6 = 16\,133$  a.u. and  $142\,129$  a.u. for KRb and RbCs, respectively; in [56],  $C_{6,00} = 13706$  a.u. for KRb is similar to our  $C_6^e + C_6^{g-e}$ . The last column illustrates the existence of two classes of molecules as noted in the text.

Molecule	Source	$C_6$ (a.u.)	$C_6^g$ (a.u.)	$C_6^e$ (a.u.)	$C_6^{g-e}$ (a.u.)	$C_6^g/C_6$ (%)
$^{23}\text{Na}^{133}\text{Cs}$	This work	7323100	7311100	9198	2800	99.8
	Ref. [38]	6946696	6932958	10822	2916	99.8
	Ref. [18]			9453	2877	
$^7\text{Li}^{133}\text{Cs}$	This work	4585400	4574400	7407	3600	99.8
	Ref. [38]	3409406	3397216	8670	3520	99.6
	Ref. [18]			7700	2920	
$^{23}\text{Na}^{87}\text{Rb}$	This work	1524900	1515800	7846	1200	99.4
	Ref. [38]	1507089	1497080	8696	1313	99.3
	Ref. [18]			7688	992	
$^7\text{Li}^{87}\text{Rb}$	This work	1252300	1244205	6314	1800	99.4
	Ref. [38]	884705	876031	6963	1711	99.0
	Ref. [18]			6193	1061	
$^{23}\text{Na}^{39}\text{K}$	This work	1070000	1070000	6323	1754	>99.0
	Ref. [38]	570190	563500	5489	1200	98.8
	Ref. [18]	411682	404491	6024	1167	99.3
$^{39}\text{K}^{133}\text{Cs}$	This work	524000	517000	6269	1241	98.7
	Ref. [38]	561070	553520	6732	800	98.7
	Ref. [18]	516606	508325	7461	820	98.4
$^{87}\text{Rb}^{133}\text{Cs}$	This work			6818	959	
	Ref. [38]	345740	329510	15619	611	95.3
	Ref. [18]	469120	450681	17716	723	96.1
$^{39}\text{K}^{87}\text{Rb}$	This work			16570	690	
	Ref. [38]	147260	129250	17707	53	87.8
	Ref. [18]	180982	160336	20301	345	88.6
$^{39}\text{K}^{87}\text{Rb}$	This work			18840	370	
	Ref. [38]	15972	3336	12576	60	20.9
	Ref. [18]	17720	3456	14202	62	19.5
$^7\text{Li}^{23}\text{Na}$	This work			13490	50	
	Ref. [38]	3583	241	3321	21	6.7
	Ref. [18]	3709	110	3582	17	3.0
$^7\text{Li}^{23}\text{Na}$	This work			3279	10	
	Ref. [38]	3880	186	3673	21	4.8
	Ref. [27]					

huge van der Waals coefficient  $C_6$ , i.e., larger than  $10^5$  a.u. The  $C_6^e$  values are comparable to those for homonuclear molecules [54], while the crossed terms  $C_6^{g-e}$  are always very weak.

Table II shows two trends: our results for  $C_6^g$  are systematically larger than the other available values (except for KRb, KCs, and RbCs from [38]), while the contrary is visible for  $C_6^e$ . Such discrepancies probably come from the sensitivity of the  $C_6$  coefficients, which scale as the fourth power of the permanent and transition dipole moments. In our calculations we use transition energies and dipole moments, averaged over rovibrational wave functions, while the other studies are done at the equilibrium distances. Those rovibrational wave functions are calculated from experimental PECs when

possible. Our underestimation of the  $C_6^e$  coefficients may be due to the slow convergence of the polarizability [Eq. (3)] with respect to the electronically excited states (and also ionization continuum), which are not all included in our calculations. The discrepancy of the  $C_6^e$  may also be related to the overestimation of the static polarizability, in particular in Ref. [38] (see Table 1 and the corresponding discussion), which is inherent in the method used by those authors. Note that the static polarizabilities obtained with the present method differ by less than 1% from the values of Ref. [10] obtained with a finite-field method. One possible way to discriminate the different theoretical calculations could be to measure collision rates, which scale, for instance, as  $C_6^{3/4}$  for identical fermionic molecules [27].

TABLE III. Various characteristic distances  $R_{vdW}$ ,  $R^*$ ,  $R_q$ , characteristic electric field  $\mathcal{E}^*$ , and position of the barrier ( $R_b$ ,  $V_b$ ) for a field  $\mathcal{E} = 1$  kV/cm (see text). The  $C_6$  coefficients (from Table II) for two identical ground-state molecules in the ( $v = 0, j = 0$ ) level are recalled for the sake of clarity.

Molecule	$C_6$ (a.u.)	$R_{vdW}$ (a.u.)	$R^*$ (a.u.)	$\mathcal{E}^*$ (kV/cm)	$R_b$ (a.u.)	$V_b$ (mK)	$R_q$ (a.u.)
$^{23}\text{Na}^{133}\text{Cs}$	7323100	574	234	0.7	328	5.3	12
$^7\text{Li}^{133}\text{Cs}$	4585400	497	178	2.0	408	0.3	10
$^{23}\text{Na}^{87}\text{Rb}$	1524900	355	175	1.3	294	0.8	16
$^7\text{Li}^{87}\text{Rb}$	1252300	325	140	3.1	428	0.06	13
$^7\text{Li}^{39}\text{K}$	570190	223	119	4.3	169	0.02	15
$^{23}\text{Na}^{39}\text{K}$	561070	240	140	2.0	327	0.1	19
$^{39}\text{K}^{133}\text{Cs}$	345740	274	156	1.0	226	0.8	38
$^{87}\text{Rb}^{133}\text{Cs}$	147260	236	148	0.8	189	1.0	60
$^{39}\text{K}^{87}\text{Rb}$	15972	118	70	4.0	451	$6 \times 10^{-4}$	109
$^7\text{Li}^{23}\text{Na}$	3583	57	31	36.1	1130	$6 \times 10^{-7}$	95

### III. MULTICHANNEL CALCULATION IN FREE SPACE

We consider in the following the eight molecules for which  $C_6^g$  is dominant (all but KRb and LiNa) as dipolar rotators characterized by  $d_0$  and  $B_0$ , ignoring the influence of the electronically excited states in their interaction.

The above single-channel description is valid down to distances  $R^* = (d_0^2/B_0)^{1/3}$  such that  $C_6/R^{*6} \approx 2B_0$ , where the dipole-dipole interaction couples the ( $j_i = 0$ ) and ( $j_i = 1$ ) levels [14]. This is easily shown using an analytical model including the two channels ( $j_1, j_2$ ) = (0,0), (1,1), namely, the basis states  $|j_1 m_1; j_2 m_2\rangle = |00; 00\rangle$ ,  $|10; 10\rangle$  and  $|1 \pm 1; 1 \mp 1\rangle$ , with  $m_i$  being the projection of  $\vec{j}_i$  on  $z$ . Defining dimensionless energies  $\bar{V} = V/B_0$  and distances  $\bar{R} = R/R^*$ , the lowest potential energy curve  $\bar{V}_{0,0}(\bar{R})$  reads

$$\bar{V}_{0,0}(\bar{R}) \approx 2 - 2\sqrt{1 + \frac{1}{6\bar{R}^6}}. \quad (5)$$

Thus  $R^*$  is the distance where the variation of  $\bar{V}_{0,0}$  suddenly changes from a variation in  $\bar{R}^{-6}$  to  $\bar{R}^{-3}$  due to the coupling with higher channels, inducing the mutual alignment of the molecules. As previously found [28], the values of  $R^*$  are about two times smaller than the vdW length  $R_{vdW}$  (Table III) where quantum reflection occurs [57,58]. We checked that this sudden change in the interaction does not modify the quantum reflection and thus the universal collision rates defined in Refs. [27,28].

The full numerical formalism must take into account the coupling between rotational levels of the diatoms induced by  $\hat{V}_{dd}$  (assuming  $v_1 = v_2 = 0$ ) by diagonalizing at each  $R$  the Hamiltonian  $\hat{H} = \hat{H}_1 + \hat{H}_2 + \hat{V}_{dd}$  in the rotational basis  $|\beta\rangle = |j_1 m_1 j_2 m_2\rangle$  and for a given parity  $p = (-1)^{j_1+j_2}$  and a given  $M = m_1 + m_2$ . The free rotation terms  $\hat{H}_i$  of molecule  $i$  only have diagonal elements equal to  $B_0 j_i(j_i + 1)$ . The matrix elements of the dipolar Hamiltonian (1) read

$$\langle \beta' | \hat{V}_{dd} | \beta \rangle = \frac{d_0^2}{R^3} C_{j_1 0}^{j_1' 0} C_{j_2 0}^{j_2' 0} \sum_q A_q C_{j_1 m_1 1 q}^{j_1' m_1'} C_{j_2 m_2 1 -q}^{j_2' m_2'}, \quad (6)$$

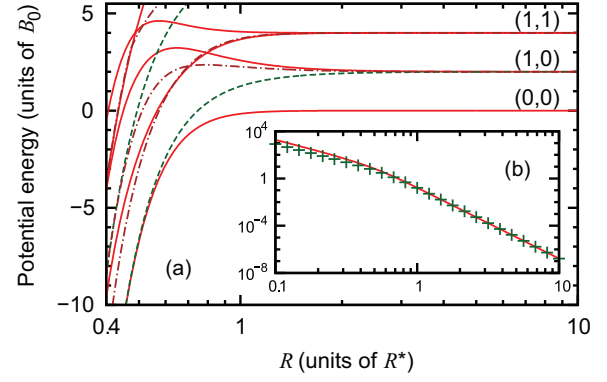


FIG. 2. (Color online) (a) Long-range adiabatic PECs (in scaled units) of  $0_g^{+(\pm)}$  (solid lines),  $0_u^{+(\pm)}$  (dashed lines), and  $1_u^{(\pm)}$  (dash-dotted lines) symmetries of two identical  $v = 0$  ground-state polar diatoms. (b) The lowest  $0_g^{+(+)}$  PEC in log scale [solid line: numerical; crosses: Eq. (5)].

where

$$A_q = -\frac{2}{(1+q)!(1-q)!} \sqrt{\frac{(2j_1+1)(2j_2+1)}{(2j_1'+1)(2j_2'+1)}} \quad (7)$$

is a numerical factor and  $C_{aabb}^{cy}$  are Clebsch-Gordan coefficients [59]. Values up to  $j_i = 6$  for  $\bar{R} > 10$ ,  $j_i = 10$  for  $0.25 < \bar{R} < 10$ , and  $j_i = 15$  for  $0.1 < \bar{R} < 0.25$  have been included in the calculations. In analogy with two atoms, the resulting adiabatic PECs are labeled  $|M|_{g/u}^{\sigma(p)}$ , where  $\sigma$  is the symmetry with respect to a plane containing the intermolecular axis.

Figure 2 displays the lowest PECs calculated numerically for the  $0_g^{+(\pm)}$ ,  $0_u^{+(\pm)}$ , and  $1_u^{(\pm)}$  symmetries, which will be relevant for the analysis in an electric field. Figure 2(b) shows that Eq. (5) correctly reproduces the full numerical calculations, although it underestimates the magnitude of the  $R^{-3}$  interaction. For  $R \gg R^*$  a one-channel description similar to the one of Sec. II is valid. The potential energy scales as  $R^{-6}$ , except for the PECs connected to the channel (1,0), which scale as  $R^{-3}$  due to the exchange of rotational excitation. As  $R \rightarrow +\infty$  the energy of the  $0_{g/u}^{+(-)}$  curves is  $\bar{V}_{1,0}(R) \approx 2 \pm 2/3\bar{R}^3$  (the + sign is for  $0_g^{+(-)}$ , and the energy of the  $1_{g/u}^{+(-)}$  curves is  $\bar{V}_{1,1}(R) \approx 2 \mp 1/3\bar{R}^3$ . For low- $R$  values ( $R \ll R^*$ ) the rotational levels become significantly coupled, giving birth, for example, to potential barriers. Finally, note the behavior of the lowest  $0_g^{+(+)}$  and  $0_u^{+(-)}$  curves, which get closer and closer when  $R$  decreases. This will have important consequences in the presence of an electric field.

### IV. APPLICATION OF AN EXTERNAL ELECTRIC FIELD

In the T-CS the influence of an external electric field on the molecule-molecule interactions is, for instance, relevant when considering experimental setups using one- or two-dimensional traps for the ultracold quantum gas. The field-molecule Hamiltonian  $\hat{W}_i = -\hat{d}_i \cdot \hat{\mathcal{E}}$  reduces to  $(-\mathcal{E} \cos \hat{\theta}_i)$  and  $(-\mathcal{E} \sin \hat{\theta}_i \cos \hat{\phi}_i)$  for parallel (along  $z$ ,  $\pi = 0 \equiv \parallel$ ) and perpendicular (along  $x$ ,  $\pi = 1 \equiv \perp$ ) fields, respectively. Its matrix elements for molecule 1 (and vice versa for molecule



2) coupling states with different parities  $p$  and  $p'$  are

$$\langle \beta' | \hat{W}_1^\pi | \beta \rangle = -\delta_{j_2 j_2'} \delta_{m_2 m_2'} \sqrt{\frac{2j_1 + 1}{2j_1' + 1}} C_{j_1 0 1 0}^{j_1' 0} \Omega_1^\pi \mathcal{E} d_0, \quad (8)$$

with

$$\Omega_1^\pi = \frac{1}{\sqrt{2(1 + \delta_{\pi 0})}} \left[ C_{j_1 m_1 1 - \pi}^{j_1' m_1'} + (-1)^\pi C_{j_1 m_1 1 \pi}^{j_1' m_1'} \right]. \quad (9)$$

The dimensionless quantity  $\bar{\mathcal{E}} = \mathcal{E}/\mathcal{E}^*$  holds for the electric field expressed in units of  $\mathcal{E}^* = B_0/d_0$  (Table III).

The electric field couples the lowest  $0_g^{+(+)}$  state  $|j_1 m_1; j_2 m_2\rangle = |00; 00\rangle$  to symmetric superpositions of  $|j_1 m_1; j_2 m_2\rangle$  and  $|j_2 m_2; j_1 m_1\rangle$  states. In the parallel case,  $|00; 00\rangle$  is directly coupled to the  $0_u^{+(-)}$  states  $|00; 10\rangle$  and  $|10; 00\rangle$ , while the latter are, in turn, directly coupled to the  $0_g^{+(+)}$  state  $|10; 10\rangle$ . Similarly, the perpendicular field induces a coupling between the  $0_g^{+(+)}$  state  $|00; 00\rangle$  and  $|00; 11\rangle$ ,  $|00; 1-1\rangle$ ,  $|11; 00\rangle$ , and  $|1-1; 00\rangle$ , which combine together to form  $1_u^{(-)}$  states [see Fig. 2(a)].

Therefore a perturbative calculation of the lowest PEC  $\bar{V}_{00;\pi}(\bar{R})$  for  $\bar{R} \gg 1$  and  $\bar{\mathcal{E}} \ll 1$  requires (i) the inclusion of the  $(j_1, j_2) = (0, 0), (1, 0), (1, 1)$  channels and (ii) the third-order correction on energy, as it contains the first crossed  $(\bar{R}, \bar{\mathcal{E}})$  contribution. In the parallel case [ $\pi = 0$  in Eq. (9)], the Hamiltonian on which the perturbation theory is applied is expressed in the basis  $|00; 00\rangle^D, (|10; 00\rangle^D + |00; 10\rangle^D)/\sqrt{2}, (|11; 1-1\rangle + |1-1; 11\rangle)/\sqrt{2}$  as

$$\begin{pmatrix} 0 & -\sqrt{2/3}\bar{\mathcal{E}} & -2/3\bar{R}^3 & -\sqrt{2/3}\bar{R}^3 \\ -\sqrt{2/3}\bar{\mathcal{E}} & 2-2/3\bar{R}^3 & -\sqrt{2/3}\bar{\mathcal{E}} & 0 \\ -2/3\bar{R}^3 & -\sqrt{2/3}\bar{\mathcal{E}} & 4 & 0 \\ -\sqrt{2/3}\bar{R}^3 & 0 & 0 & 4 \end{pmatrix}. \quad (10)$$

It gives for the lowest PEC

$$\bar{V}_{00;\parallel}(\bar{R}, \bar{\mathcal{E}}) \approx -\frac{2\bar{\mathcal{E}}^2}{9\bar{R}^3} - \frac{1}{6\bar{R}^6}, \quad (11)$$

where the energy of the two infinitely separated molecules has been set to zero for each  $\bar{\mathcal{E}}$ . The attractive  $R^{-3}$  character of the lowest PEC, induced by the head-to-tail configuration of the two molecules, is valid only for distances such that  $\bar{R} \gg \bar{\mathcal{E}}^{-2/3}$ , while below this limit the vdW term is dominant.

In the perpendicular case [ $\pi = 1$  in Eq. (9)] a similar perturbative calculation gives for the lowest PEC

$$\bar{V}_{00;\perp}(\bar{R}, \bar{\mathcal{E}}) \approx \frac{\bar{\mathcal{E}}^2}{9\bar{R}^3} - \frac{1}{6\bar{R}^6}. \quad (12)$$

The ‘‘huge’’ vdW term competes with a side-by-side repulsive  $R^{-3}$  term, resulting in an expected potential barrier located at

$$\bar{R}_b \approx (3/\bar{\mathcal{E}}^2)^{1/3}, \quad (13)$$

with the height

$$\bar{V}_b \approx \bar{\mathcal{E}}^4/54. \quad (14)$$

In physical units the coordinates of the barrier are  $R_b \approx (3B_0/\mathcal{E}^2)^{1/3}$  and  $V_b \approx d_0^4 \mathcal{E}^4/54B_0^3$ . As  $\mathcal{E}$  increases, the barrier shifts toward low  $R$ , but its height remains small compared to  $B_0$ , even for moderate fields  $\bar{\mathcal{E}} \approx 1$ . The position and height of the barrier, calculated for an electric field of 1 kV/cm, are given in Table III for each species. The height increases with

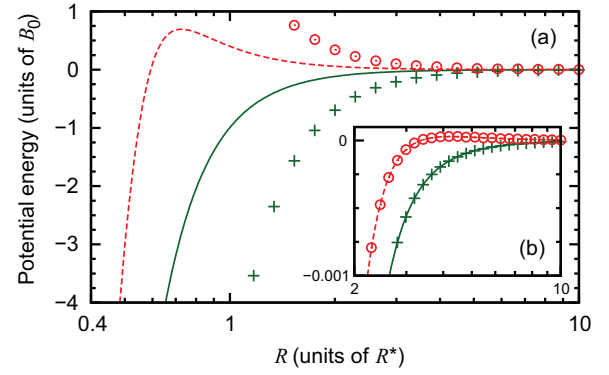


FIG. 3. (Color online) Long-range adiabatic PECs (in scaled units) for two identical  $v = 0$  ground-state polar diatoms submitted to an external electric field: (a)  $\mathcal{E} = 5\mathcal{E}^*$  and (b)  $\mathcal{E} = \mathcal{E}^*/5$ . The solid (dashed) lines correspond to the numerical results in a parallel (perpendicular) field. The plus signs (open circles) correspond to the analytical approximations [Eqs. (11) and (12)] in a parallel (perpendicular) field.

the molecular dipole moment, so that colliding molecules like NaCs are unlikely to overcome the barrier in the ultracold regime. Figure 3 shows that these features are observable in the PECs obtained after the diagonalization of the molecule-molecule plus molecule-field Hamiltonians [Eqs. (6) and (8)]. For a weak field [Fig. 3(b)] the perturbative expressions (11) and (12) are in very good agreement with the numerical results. In the strong-field regime [Fig. 3(a)], i.e., outside the perturbative regime, Eq. (12) captures the essential features of the numerical results, even if the height of the potential barrier calculated numerically is smaller due to the coupling with higher levels, which are not included in the analytical estimate.

The lowest PEC can be conveniently and unambiguously characterized by the leading exponent  $n^*(\bar{R}, \bar{\mathcal{E}})$  of the long-range interaction

$$n^*(\bar{R}, \bar{\mathcal{E}}) = \frac{\partial \log_{10} |V_{00;\pi}(\bar{R}, \bar{\mathcal{E}})|}{\partial \log_{10} \bar{R}}, \quad (15)$$

with  $n^* = -3$  if the interaction is of the pure dipole-dipole type and  $n^* = -6$  if it is of the pure vdW type. In Fig. 4,  $n^*$  is plotted as a function of  $\bar{R}$  and  $\bar{\mathcal{E}}$  for parallel and perpendicular fields. Figures 4(a) and 4(b) correspond to KRb but are also applicable to LiNa, while Figs. 4(c) and 4(d) correspond to the eight other molecules. The  $(\bar{R}, \bar{\mathcal{E}})$  plane is divided in different areas labeled with Roman numerals.

In region I the van der Waals interaction dominates the dipolar interaction even in nonvanishing fields. Region III corresponds to the expected dipole-dipole interaction, which is attractive due to a head-to-tail approach in a parallel field and repulsive due to a side-by-side approach in a perpendicular field. Region III spreads to the low- $R$  values with increasing fields, and its border with region I scales as  $\mathcal{E} \sim R^{-3/2}$ , as predicted from Eqs. (11) and (12). In a perpendicular field the competition between the repulsive dipole-dipole interaction and the attractive vdW interaction (represented by the + and - signs in Figs. 4(b) and 4(d)) induces a change in the sign of the potential energy, which causes the divergence of  $n^*$ .

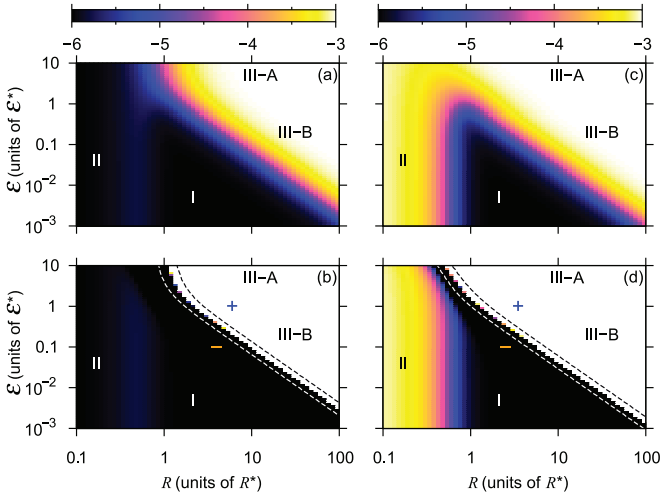


FIG. 4. (Color online) Leading exponent  $n^*$  [Eq. (15)] characterizing the molecule-molecule interaction for the lowest state in parallel (top row) and perpendicular (bottom row) electric fields in the T-CS as a function of  $R$  and  $\mathcal{E}$  in reduced units: (a) and (b) for KRb and (c) and (d) for all species except KRb and LiNa. The color scale ranges from black ( $n^* = -6$ ) to white ( $n^* = -3$ ). The Roman numerals correspond to regions of the  $(R, \mathcal{E})$  plane characterized by different types of interactions (see text). In (b) and (d) the + (−) symbol refers to a repulsive (attractive) interaction, while the zones between the dashed lines correspond to a change of sign of the interaction and are physically irrelevant (see text).

In Figs. 4(b) and 4(d), the region between the dotted lines is physically irrelevant due to this divergence.

Region II in Figs. 4(c) and 4(d) is characterized by a dominant dipole-dipole interaction in  $R^{-3}$ , as expected for the most polar molecules. Region II even exists at  $\bar{\mathcal{E}} = 0$ , as observed on Fig. 2, and its border with region I is field independent. The dipole-dipole interaction strongly couples the rotational levels of the molecules, which causes their mutual orientation. For KRb [Figs. 4(a) and 4(b)], an approximate value of  $n^*$  is obtained by diagonalizing Eq. (6) in physical units and adding the diagonal contribution  $-(C_6^{g-e} + C_6^e)/R^6$ . It is striking to see that while regions I and III are similar to those of the former case, the vdW interaction dominates even at short distances (region II) even at high electric fields due to the low value of the PEDM.

## V. DISCUSSION: ALIGNMENT AND ORIENTATION OF INTERACTING POLAR MOLECULES

In order to understand more deeply the interaction between the eight most polar molecules, we also calculated the induced dipole moment  $\bar{d}_i(\bar{R}, \bar{\mathcal{E}})$  (in units of  $d_0$ ) along the electric-field axis,

$$\bar{d}_i(\bar{R}, \bar{\mathcal{E}}) = \langle \hat{d}_i \cdot \hat{\mathcal{E}} \rangle, \quad (16)$$

and the mutual alignment of the two molecules  $s(\bar{R}, \bar{\mathcal{E}})$ , expressed as the scalar product

$$s(\bar{R}, \bar{\mathcal{E}}) = \langle \hat{d}_1 \cdot \hat{d}_2 \rangle, \quad (17)$$

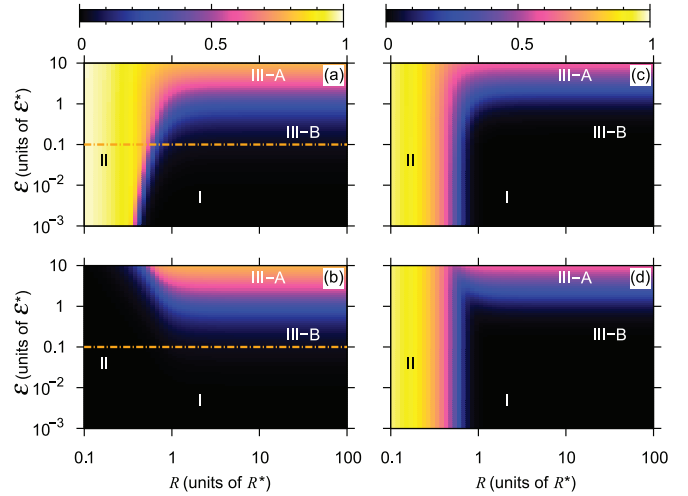


FIG. 5. (Color online) The molecule-molecule interaction for the lowest state in parallel (top row) and perpendicular (bottom row) electric fields in the T-CS as a function of  $R$  and  $\mathcal{E}$  in reduced units. The color scale ranges from black (minimal values) to white (maximal values). (a) and (b) Induced dipole moment  $\bar{d}_i$  of molecule  $i$  ( $i = 1$  or 2) along the field axis [Eq. (16)]; (c) and (d) scalar product  $s$  of the two dipole moments [Eq. (17)]. The Roman numerals correspond to regions of the  $(R, \mathcal{E})$  plane characterized by different types of interactions (see text). The horizontal line in (a) and (b) drawn at  $\mathcal{E} = \mathcal{E}^*/10$  locates the regime for which the variation of the induced dipole moment is discussed in the text.

where  $\langle \cdot \cdot \rangle$  denotes the average over the eigenvector associated with the lowest PEC. The quantities  $\bar{d}_i$  and  $s$  are plotted on Fig. 5, which features the same regions as Fig. 4.

In region I, both  $\bar{d}_i$  and  $s$  vanish: in a simple picture the dominant vdW interaction can be regarded as the consequence of the independent rotation of the two molecules. Although region III displays the expected  $R^{-3}$  dipolar interaction, Fig. 5 shows that for low fields ( $\bar{\mathcal{E}} < 1$ , region III-B) the dipoles are not aligned along the field and average to zero, nor are they aligned against each other. The inverted situation takes place at high fields ( $\bar{\mathcal{E}} > 1$ , region III-A). The molecular alignment becomes significant for  $\bar{\mathcal{E}} \sim 1$ , i.e.,  $\mathcal{E} \sim \mathcal{E}^*$ . In Table III we see that  $\mathcal{E}^*$  decreases with the PEDM magnitude. This means that the molecules interacting with the strongest vdW force are actually the easiest to align along the field.

Figures 5(c) and 5(d) show that in region II the molecules are aligned with respect to each other in a head-to-tail configuration ( $s \approx 1$ ), while there is no preferential orientation ( $\bar{d}_i = 0$ ) in a perpendicular field. The large dipole-dipole interaction, compared to the Stark energy, strongly correlates the molecules to each other, whereas they are not influenced by the field. Surprisingly, in a parallel field, both  $s$  and  $\bar{d}_i$  are close to unity, which reflects a strong molecular alignment even at small fields [see Fig. 5(a)]. This comes from the degeneracy between the lowest  $0_g^{+(+)}$  and  $0_u^{+(-)}$  field-free PECs visible in Fig. 2(a). A small field is sufficient to raise that degeneracy, and the lower of the resulting states is very efficiently aligned along the field (while the upper one, not shown here, is antialigned, i.e.,  $\bar{d}_i \approx -1$ ).

For a moderate parallel field, say  $\mathcal{E} = \mathcal{E}^*/10$  as illustrated by the dashed line in Figs. 5(a) and 5(c), the dipole moment

strongly varies with  $R$ : it changes from  $\bar{d}_i = 0.18$  at  $\bar{R} = 0.74$  up to  $\bar{d}_i = 0.81$  at  $\bar{R} = 0.45$ . For the five species (NaK, NaRb, NaCs, KCs, and RbCs) among the ten heteronuclear bialkali molecules which are found to be stable against ground-state collisions [60], this feature suggests that the formation of ultracold polar tetramers could be possible by a stimulated one-photon radiative association process along the lines proposed in Ref. [61].

In contrast, such an association process cannot occur when the electric field is perpendicular to the intermolecular axis since the individual dipole moments  $\bar{d}_i$  are zero. Thus we predict that this mechanism is strongly anisotropic and that electric fields could be used to control the association of the tetramers, in a similar way to the one used to reduce the collision rate of ultracold KRb molecules in the JILA experiment.

## VI. CONCLUSIONS

In this article, we compute the long-range interactions, in free space and in an external electric field, between two identical ground-state heteronuclear bialkali molecules for the ten species composed of Li, Na, K, Rb, and Cs atoms. We find two distinct groups of molecules: on the one hand, eight possess a permanent electric dipole moment larger than 1 D, and on the other hand, LiNa and KRb possess a weak permanent electric dipole moment. For the eight most polar molecules, the long-range interactions are analyzed in terms of scaled intermolecular distances, electric field, and energy, which are constructed from the dipole moment and rotational constant in the vibrational ground level.

The most polar molecules interact through a huge van der Waals force, up to three orders of magnitude larger than for homonuclear molecules or atoms. For distances  $R$  roughly smaller than 100 a.u., this van der Waals interaction turns into a dipole-dipole interaction due to the mutual orientation of the two molecules. Although this change in behavior occurs at a distance  $R^*$  of the same order of magnitude as the van der Waals length  $R_{\text{vdW}}$ , we have checked that it does not alter the universal collision rates for reactive species [27,28]. In the

case of LiNa and KRb, the smaller- $R$  mutual orientation does not happen because of the weak permanent electric dipole moment.

When the field is turned on, the expected dipole-dipole interaction is observed for the ten molecules for electric-field magnitudes larger than a certain threshold value. Except for LiNa, this value is accessible in current ultracold experiments. In the region of mutual orientation and for an electric field parallel to the intermolecular axis, we predict a very strong alignment of the molecules along the field axis which is due to a surprising degeneracy between two curves significantly coupled by the field. The resulting strongly  $R$ -varying induced dipole moment suggests the possibility of a controlled one-photon stimulated association of ultracold ground-state polar tetramers.

In Ref. [18] the authors compute the terms of the multipolar expansion from  $R^{-3}$  to  $R^{-8}$  for two polar bialkali molecules with fixed distances and angles. Then those purely electronic terms are averaged on electric-field-dressed rotational levels of each molecule for different intermolecular distances. It is shown that the quadrupole-quadrupole interaction scaling as  $R^{-5}$  dominates the dipole-dipole interaction for distances lower than  $R_q$  (last column of Table III). For the six most polar molecules,  $R_q$  is smaller than 20 a.u., where our model is no longer valid. For LiNa, KRb, RbCs, and KCs, this interaction may play a significant role in the small- $R$  region [17,18], but it would require a separate study for each molecule.

## ACKNOWLEDGMENTS

Enlightening discussions with Goulven Quéméner, Piotr Zuchowski, Jason Byrd, and Robin Côté are gratefully acknowledged. This work was supported in part by Triangle de la Physique (Contract No. 2008-007T-QCCM) and by the National Science Foundation (Grant No. NSF PHY11-25915). We acknowledge the computing facility GMPCS of the LUMAT federation (FR LUMAT 2764). Laboratoire Aimé Cotton is a member of the Institut Francilien de Recherches sur les Atomes Froids.

- 
- [1] L. D. Carr and J. Ye, *New J. Phys.* **11**, 055009 (2009).
  - [2] O. Dulieu and C. Gabbanini, *Rep. Prog. Phys.* **72**, 086401 (2009).
  - [3] D. Blume, *Rep. Prog. Phys.* **75**, 046401 (2012).
  - [4] I. Bloch, J. Dalibard, and S. Nascimbène, *Nat. Phys.* **8**, 267 (2012).
  - [5] V. Galitski and I. B. Spielman, *Nature (London)* **494**, 49 (2013).
  - [6] T. Lahaye, C. Menotti, L. Santos, M. Lewenstein, and T. Pfau, *Rep. Prog. Phys.* **72**, 126401 (2009).
  - [7] B. Pasquiou, E. Maréchal, L. Vernac, O. Gorceix, and B. Laburthe-Tolra, *Phys. Rev. Lett.* **108**, 045307 (2012).
  - [8] M. de Miranda, A. Chotia, B. Neyenhuis, D. Wang, G. Quéméner, S. Ospelkaus, J. Bohn, J. Ye, and D. Jin, *Nat. Phys.* **7**, 502 (2011).
  - [9] K.-K. Ni, S. Ospelkaus, M. H. G. de Miranda, A. Peer, B. Neyenhuis, J. J. Zirbel, S. Kotochigova, P. S. Julienne, D. S. Jin, and J. Ye, *Science* **322**, 231 (2008).
  - [10] J. Deiglmayr, M. Aymar, R. Wester, M. Weidemüller, and O. Dulieu, *J. Chem. Phys.* **129**, 064309 (2008).
  - [11] S. Ospelkaus, K.-K. Ni, G. Quéméner, B. Neyenhuis, D. Wang, M. H. G. de Miranda, J. L. Bohn, J. Ye, and D. S. Jin, *Phys. Rev. Lett.* **104**, 030402 (2010).
  - [12] A. V. Avdeenkov and J. L. Bohn, *Phys. Rev. A* **66**, 052718 (2002).
  - [13] A. V. Avdeenkov and J. L. Bohn, *Phys. Rev. Lett.* **90**, 043006 (2003).
  - [14] A. Micheli, G. Pupillo, H. P. Büchler, and P. Zoller, *Phys. Rev. A* **76**, 043604 (2007).
  - [15] L. Holmegaard, J. H. Nielsen, I. Nevo, H. Stapelfeldt, F. Filsinger, J. Küpper, and G. Meijer, *Phys. Rev. Lett.* **102**, 023001 (2009).
  - [16] J. Nielsen, H. Stapelfeldt, J. Küpper, B. Friedrich, J. J. Omiste, and R. González-Férez, *Phys. Rev. Lett.* **108**, 193001 (2012).

- [17] J. Byrd, J. A. Montgomery, Jr., and R. Côté, *Phys. Rev. Lett.* **109**, 083003 (2012).
- [18] J. N. Byrd, J. A. Montgomery, Jr., and R. Côté, *Phys. Rev. A* **86**, 032711 (2012).
- [19] S. Ospelkaus, K.-K. Ni, D. Wang, M. H. G. de Miranda, B. Neyenhuis, G. Quéméner, P. S. Julienne, J. Bohn, D. S. Jin, and J. Ye, *Science* **327**, 853 (2010).
- [20] P. Julienne, *Faraday Discuss.* **142**, 361 (2009).
- [21] Z. Idziaszek and P. S. Julienne, *Phys. Rev. Lett.* **104**, 113202 (2010).
- [22] G. Quéméner and J. L. Bohn, *Phys. Rev. A* **81**, 022702 (2010).
- [23] G. Quéméner and J. L. Bohn, *Phys. Rev. A* **81**, 060701(R) (2010).
- [24] W. C. Stwalley, J. Banerjee, M. Bellos, R. Carollo, M. Recore, and M. Mastroianni, *J. Phys. Chem. A* **114**, 81 (2010).
- [25] P. Zabawa, A. Wakim, A. Neukirch, C. Haimberger, N. P. Bigelow, A. V. Stolyarov, E. A. Pazyuk, M. Tamanis, and R. Ferber, *Phys. Rev. A* **82**, 040501 (2010).
- [26] M. Debatin, T. Takekoshi, R. Rameshan, L. Reichsoellner, F. Ferlaino, R. Grimm, R. Vexiau, N. Bouloufa, O. Dulieu, and H.-C. Nägerl, *Phys. Chem. Chem. Phys.* **13**, 18926 (2011).
- [27] G. Quéméner, J. L. Bohn, A. Petrov, and S. Kotochigova, *Phys. Rev. A* **84**, 062703 (2011).
- [28] P. Julienne, T. Hanna, and Z. Idziaszek, *Phys. Chem. Chem. Phys.* **13**, 19114 (2011).
- [29] T. Takekoshi, M. Debatin, R. Rameshan, F. Ferlaino, R. Grimm, H.-C. Nägerl, C. Le Sueur, J. Hutson, P. Julienne, S. Kotochigova, and E. Tiemann, *Phys. Rev. A* **85**, 032506 (2012).
- [30] C.-H. Wu, J. W. Park, P. Ahmadi, S. Will, and M. W. Zwierlein, *Phys. Rev. Lett.* **109**, 085301 (2012).
- [31] M. Repp, R. Pires, J. Ulmanis, R. Heck, E. D. Kuhnle, M. Weidemüller, and E. Tiemann, *Phys. Rev. A* **87**, 010701(R) (2013).
- [32] S.-K. Tung, C. Parker, J. Johansen, C. Chin, Y. Wang, and P. S. Julienne, *Phys. Rev. A* **87**, 010702(R) (2013).
- [33] M. Lepers, O. Dulieu, and V. Kokoouline, *Phys. Rev. A* **82**, 042711 (2010).
- [34] M. Lepers, R. Vexiau, N. Bouloufa, O. Dulieu, and V. Kokoouline, *Phys. Rev. A* **83**, 042707 (2011).
- [35] M. Lepers and O. Dulieu, *Eur. Phys. J. D* **65**, 113 (2011).
- [36] M. Lepers and O. Dulieu, *Phys. Chem. Chem. Phys.* **13**, 19106 (2011).
- [37] M. Lepers, B. Bussery-Honvault, and O. Dulieu, *J. Chem. Phys.* **137**, 234305 (2012).
- [38] P. S. Żuchowski, M. Kosicki, M. Kodrycka, and P. Soldán, *Phys. Rev. A* **87**, 022706 (2013).
- [39] M. Aymar and O. Dulieu, *J. Chem. Phys.* **122**, 204302 (2005).
- [40] A. Derevianko, S. Porsev, and J. Babb, *At. Data Nucl. Data Tables* **96**, 323 (2010).
- [41] M. Aymar and O. Dulieu, *Mol. Phys.* **105**, 1733 (2007).
- [42] V. Kokoouline, O. Dulieu, R. Kosloff, and F. Masnou-Seeuws, *J. Chem. Phys.* **110**, 9865 (1999).
- [43] R. Vexiau, Ph.D. thesis, Université Paris-Sud, 2012.
- [44] O. Docenko, M. Tamanis, R. Ferber, A. Pashov, H. Knöckel, and E. Tiemann, *Eur. Phys. J. D* **31**, 205 (2004).
- [45] P. Staantum, A. Pashov, H. Knöckel, and E. Tiemann, *Phys. Rev. A* **75**, 042513 (2007).
- [46] O. Docenko, M. Tamanis, R. Ferber, A. Pashov, H. Knöckel, and E. Tiemann, *Phys. Rev. A* **69**, 042503 (2004).
- [47] M. Ivanova, A. Stein, A. Pashov, H. Knöckel, and E. Tiemann, *J. Chem. Phys.* **134**, 024321 (2011).
- [48] E. Tiemann, H. Knöckel, P. Kowalczyk, W. Jastrzebski, A. Pashov, H. Salami, and A. J. Ross, *Phys. Rev. A* **79**, 042716 (2009).
- [49] A. Gerdes, M. Hobein, H. Knöckel, and E. Tiemann, *Eur. Phys. J. D* **49**, 67 (2008).
- [50] R. Ferber, I. Klincare, O. Nikolayeva, M. Tamanis, H. Knöckel, E. Tiemann, and A. Pashov, *Phys. Rev. A* **80**, 062501 (2009).
- [51] O. Docenko, M. Tamanis, R. Ferber, H. Knöckel, and E. Tiemann, *Phys. Rev. A* **83**, 052519 (2011).
- [52] A. Pashov, O. Docenko, M. Tamanis, R. Ferber, H. Knöckel, and E. Tiemann, *Phys. Rev. A* **76**, 022511 (2007).
- [53] C. Fellows, *J. Mol. Spec.* **136**, 369 (1989).
- [54] J. Byrd, R. Côté, and J. Montgomery, Jr., *J. Chem. Phys.* **135**, 244307 (2011).
- [55] S. Kotochigova, *New J. Phys.* **12**, 073041 (2010).
- [56] A. Buchachenko, A. Stolyarov, M. Szczęśniak, and G. Chałasiński, *J. Chem. Phys.* **137**, 114305 (2012).
- [57] P. Julienne and F. Mies, *J. Opt. Soc. Am. B* **6**, 2257 (1989).
- [58] C. J. Williams, E. Tiesinga, P. S. Julienne, H. Wang, W. C. Stwalley, and P. L. Gould, *Phys. Rev. A* **60**, 4427 (1999).
- [59] D. A. Varshalovich, A. N. Moskalev, and V. K. Khersonskii, *Quantum Theory of Angular Momentum* (World Scientific, Singapore, 1988).
- [60] P. S. Żuchowski and J. M. Hutson, *Phys. Rev. A* **81**, 060703(R) (2010).
- [61] E. Juarros, P. Pellegrini, K. Kirby, and R. Côté, *Phys. Rev. A* **73**, 041403 (2006).